



P2X3-selective mechanism of Gefapixant, a drug candidate for the treatment of refractory chronic cough

Wen-Wen Cui^{a,b,1}, Si-Yu Wang^{a,1}, Yu-Qing Zhang^{a,1}, Yao Wang^e, Ying-Zhe Fan^c, Chang-Run Guo^a, Xing-Hua Li^a, Yun-Tao Lei^a, Wen-Hui Wang^a, Xiao-Na Yang^a, Motoyuki Hattori^e, Chang-Zhu Li^{d,*}, Jin Wang^{a,*}, Ye Yu^{a,b,*}

^aSchool of Basic Medicine and Clinical Pharmacy and State Key Laboratory of Natural Medicines, China Pharmaceutical University, Nanjing 210009, China

^bDepartment of Pharmacology and Chemical Biology, Institute of Medical Sciences, Shanghai Jiao Tong University School of Medicine, Shanghai 200025, China

^cPutuo Hospital, Shanghai University of Traditional Chinese Medicine, Shanghai 200025, China

^dState Key Laboratory of Utilization of Woody Oil Resource, Hunan Academy of Forestry, Changsha 410004, China

^eState Key Laboratory of Genetic Engineering, Collaborative Innovation Center of Genetics and Development, Shanghai Key Laboratory of Bioactive Small Molecules, Department of Physiology and Neurobiology, School of Life Sciences, Fudan University, Shanghai 200438, China

ARTICLE INFO

Article history:

Received 3 November 2021

Received in revised form 16 March 2022

Accepted 27 March 2022

Available online 31 March 2022

Keywords:

Gefapixant/AF-219

P2X3 receptors

Refractory chronic cough

Binding sites

Subtype selectivity

ABSTRACT

Gefapixant/AF-219, a selective inhibitor of the P2X3 receptor, is the first new drug other than dextromethorphan to be approved for the treatment of refractory chronic cough (RCC) in nearly 60 years. To date, seven P2X subtypes (P2X1-7) activated by extracellular ATP have been cloned, and subtype selectivity of P2X inhibitors is a prerequisite for reducing side effects. We previously identified the site and mechanism of action of Gefapixant/AF-219 on the P2X3 receptor, which occupies a pocket consisting of the left flipper (LF) and lower body (LB) domains. However, the mechanism by which AF-219 selectively acts on the P2X3 receptor is unknown. Here, we combined mutagenesis, chimera construction, molecular simulations, covalent occupation and chemical synthesis, and find that the negative allosteric site of AF-219 at P2X3 is also present in other P2X subtypes, at least for P2X1, P2X2 and P2X4. By constructing each chimera of AF-219 sensitive P2X3 and insensitive P2X2 subtypes, the insensitive P2X2 subtype was made to acquire the inhibitory properties of AF-219 and AF-353, an analog of AF-219 with higher affinity. Our results suggest that the selectivity of AF-219/AF-353 for P2X3 over the other P2X subtypes is determined by a combination of the accessibility of P2X3 binding site and the internal shape of this pocket, a finding that could provide new perspectives for drug design against P2X3-mediated diseases such as RCC, idiopathic pulmonary fibrosis, hypertension and overactive bladder disorder.

© 2022 The Authors. Published by Elsevier B.V. on behalf of Research Network of Computational and Structural Biotechnology. This is an open access article under the CC BY-NC-ND license (<http://creativecommons.org/licenses/by-nc-nd/4.0/>).

1. Introduction

P2X receptors are an important class of ATP-gated trimeric ion channels, and seven homotrimers or heterotrimers of P2X1-7 have been identified in most tissues [1]; they are implicated in a variety

of physiological and pathological functions such as synaptic transmission, sensory perception, muscle contraction, pain, thrombosis and immune regulation, and therefore are an important class of new drug targets [2]. Although there is no specific drug that is currently available for clinical treatments, a few small molecules targeting P2X3, P2X4 and P2X7 have been identified, especially those targeting P2X3 and P2X7, which have shown significant efficacy in the clinical trials [1,3]. For example, Gefapixant (AF-219), an antagonist of the P2X3 receptor, has shown significant efficacy in refractory chronic cough (RCC) and is the first new drug other than dextromethorphan to be approved for the treatment of RCC in the last 60 years [4-9]. Similarly, other P2X3 antagonists BAY-1817080 [10,11], BAY-1902607 [12], BLU-5937 [13,14] and S-600918 [15,16] are all being studied in phase II or phase III clinical

Abbreviations: RCC, refractory chronic cough; LF, left flipper; LB, lower body; IC₅₀, the concentration yielding half of the maximal inhibition; DF, dorsal fin; NPM, N-phenylmaleimide; MD, molecular dynamics.

* Corresponding authors at: School of Basic Medicine and Clinical Pharmacy and State Key Laboratory of Natural Medicines, China Pharmaceutical University, Nanjing 210009, China.

E-mail addresses: lichangzhu2013@aliyun.com (C.-Z. Li), wangjin@cpu.edu.cn (J. Wang), yuye@cpu.edu.cn (Y. Yu).

¹ Equal contributions to this work.

<https://doi.org/10.1016/j.csbj.2022.03.030>

2001-0370/© 2022 The Authors. Published by Elsevier B.V. on behalf of Research Network of Computational and Structural Biotechnology.

This is an open access article under the CC BY-NC-ND license (<http://creativecommons.org/licenses/by-nc-nd/4.0/>).

trials as treatment for RCC. Outside of the respiratory system, the P2X3 receptor antagonist BAY-1817080 is being used to treat endometriosis [17] and overactive bladder disorder [18]. The P2X4 receptor antagonist NC-2600 is in phase I clinical trials for the treatment of neuropathic pain [19], and has shown promising data in the treatment of chronic cough without taste disturbance [20]. Several P2X7 antagonists being investigated for the treatment of rheumatoid arthritis (CE-224,535 [21], EVT 401 [22] and AZD 9056 [23,24]), inflammation (GSK-1482160 [25,26]), neuropathic pain (AFC-5128 [27] and RQ-00466479 [28]), major depressive disorder (JNJ-54175446 [29,30]), mood disorder (JNJ-55308942 [31,32]), multiple sclerosis and gastrocnemius dystrophy (AFC-5128 [27]), respectively, are in phase I and phase II clinical trials.

The difficulties in the development of selective drugs targeting P2X receptors are mainly due to the following aspects: *First*, P2X subtypes involved in the regulation of different physiological functions are distributed in different tissues and organs, and effective P2X subtype selectivity is essential to reduce the side effect of drugs. However, highly conserved sequence of P2X receptors make subtype selectivity a challenge for drug discovery [1]. For example, P2X4 antagonists containing carbamazepine scaffolds have a stable and pronounced inhibitory effect on human P2X4 (hP2X4), in addition to hP2X1, hP2X3 and hP2X7 [33]. *Second*, the highly conserved amino acids at the ATP-binding pocket limit the specificity of orthosteric modulators, making the development of selective orthosteric modulators extremely difficult [34]. The commonly used competitive inhibitor TNP-ATP has strong effects on both P2X1 and P2X3, and weak effects on P2X2 and P2X4 [35,36]. *Third*, subtle sequence differences between the human- and rodent-derived P2X receptors make some subtype-selective drug molecules troublesome with species differences, which hinders the exploration of drugs in model animals and human clinical trials. For example, the antagonist of P2X3 receptors, RO-51, has much stronger affinity for rodents than for human P2X3, while carbamazepine-like antagonists of the P2X4 receptor and BX430 are both more effective against hP2X4 and less effective or ineffective against rodent P2X4 [33,37]. GW791343, a molecule targeting P2X7 receptors, has an opposite effect on human and murine P2X7 [38].

AF-219 (IC_{50} , the concentration yielding half of the maximal inhibition, = 42.6 ± 2.9 nM) and AF-353 (IC_{50} = 9.9 ± 1.1 nM), two compounds with the same structural core (see below, Fig. 7), are negative allosteric modulators specifically targeting P2X3 receptors (with IC_{50} values >10 μ M on P2X1, P2X2, P2X4, P2X5 and P2X7) [39–41]. We identified a mechanism by which the binding of these two compounds prevented the movement of the left flipper (LF) domain and thus exerted an inhibitory effect [42]. However, the structural basis for the selectivity of AF-219 and AF-353 in the highly homologous P2X subtypes remains unexplored, an issue that is critical for drug discovery of the P2X receptor.

Here, we investigated the mechanism for the generation of P2X3 subtype and species specificity of these two allosteric small molecules through chimera construction, click chemical covalent modification of proteins, structural modification of AF-353/AF-219, and dynamic analysis of protein-small molecule interactions. We found that: 1. pocket accessibility and access pathways are extremely important for drug accessibility and species differences; 2. the matching of pocket internal shape to small molecule drugs significantly affects the binding and action of the small molecule drug; 3. subtle differences in pocket overall structure between different P2X receptor subtypes are also involved in the determination of drug action specificity. Meanwhile, we further confirmed our findings by integrating various potential influencing factors into the chimera to obtain the ability of AF-219/AF-353 inhibition using the AF-219/AF-353 insensitive P2X2 subtype as an example.

Our study on the subtype specificity of AF-219/AF-353 will provide new perspectives for further RCC drug designs.

2. Materials and methods

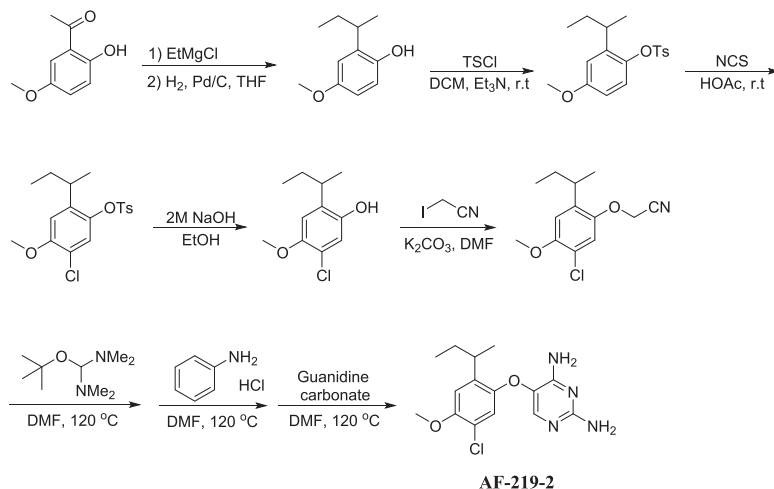
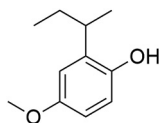
2.1. Molecular and cell biology

The rat P2X2 (rP2X2), rat P2X3 (rP2X3), rat P2X4 (rP2X4) and rat P2X7 (rP2X7) plasmids were kindly gifted by Drs. Alan North and Lin-Hua Jiang. The human P2X1 (hP2X1) cDNA was synthesized by Gikai Gene and subcloned by us into the pcDNA3.1 vector. Chicken P2X3 (cP2X3) plasmid was synthesized and subcloned into pEGFP-N1 by Beijing Genomics Institute (BGI). Mutants and chimeras were constructed by KOD-Plus mutagenesis kit (Toyobo) and confirmed by DNA sequencing. HEK293 cells were bought from Cell Bank, Shanghai Institutes for Biological Sciences, Chinese Academy of Sciences. The cells were cultured in medium containing 88% Dulbecco's Modified Eagle Medium (DMEM) (Corning), 10% fetal bovine serum (FBS) (PAN), 1% Glutamax (Gibco) and 1% penicillin/streptomycin (HyClone) at 37 °C in a humidified atmosphere of 5% CO₂ and 95% air. Plasmids were transfected into HEK293 cells by calcium phosphate transfection [43]. In brief, 2.5 μ g plasmid DNA was mixed directly with 100 μ L 0.25 M CaCl₂ solution and then mixed slowly into 2 \times HBS solution to ensure the formation of calcium phosphate-DNA precipitate. 2 \times HBS solution contains (in mM) 140 NaCl, 1.5 Na₂HPO₄, 50 HEPES, and the pH is adjusted to 6.96.

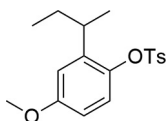
2.2. Electrophysiological recordings

Conventional whole-cell and nystatin-perforated patch-clamp recording methods were used at room temperature (25 ± 2 °C) [44–47]. The electrophysiological measurements were performed 24–48 h after transfection. The resistance of patch pipettes was 3–5 megohms ($m\Omega$) pulled from glass capillaries on a two-stage puller (PC-100, Narishige) when filled with the pipette solution contains (in mM) 120 KCl, 30 NaCl, 1 MgCl₂·6H₂O, 0.5 CaCl₂·2H₂O, 10 HEPES and 5 EGTA adjusted to pH 7.35–7.40. The bath solution contains (in mM) 150 NaCl, 0.5 KCl, 10 glucose, 2 CaCl₂·2H₂O, 10 HEPES and 1 MgCl₂·6H₂O adjusted to pH 7.35–7.40. For nystatin-perforated patch-clamp recording, the pipette solution contains (in mM) 75 K₂SO₄, 55 KCl, 5 MgSO₄ and 10 HEPES, pH 7.2. Membrane currents were measured using an Axon patch 200B patch clamp amplifier (Molecular Devices, USA). A low-pass Bessel filter was used to filter currents at 2 kHz. All currents were digitized using a Digidata 1550B interface and pCLAMP software (Molecular Devices). The membrane potential was held at -60 mV. To avoid the rundown of currents in multi-dose applications of ATP, nystatin (0.15 mg/mL)-perforated patch clamp technique was used with application intervals of saturated-concentration ATP at about 8 min, which recording was discarded when current amplitudes in respond to the first two ATP applications varied more than 20%. Currents of rP2X2 and rP2X7 receptors were recorded by conventional whole-cell patch configuration, while other subtypes were recorded by nystatin-perforated recordings. Electrophysiological recordings were repeated at least 3 times for each mutation or for each concentration of the drug, and these independent experiments are derived from cells transfected at least 2–3 times on different days. Data were normalized to the average value of the first two ATP-evoked currents. All inhibitors were pre-applied for 1 min and then co-applied with the agonist. N-phenylmaleimide (NPM) was diluted to ~ 0.5 –1 mM and immediately perfused to the cell membrane for 5 min and 2 min, respectively. AF-353 was purchased from Sigma-Aldrich, and AF-219 and AF-219-1 were synthesized according to our previous description [42].

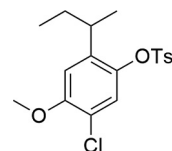
2.3. Chemical synthesis of AF-219-2

2.3.1. 2-(*sec*-butyl)-4-methoxyphenol

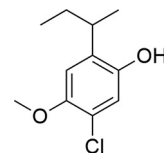
Following the prepare procedure of 2-isopropyl-4-methoxyphenol described in our previous work [42], 2-(*sec*-butyl)-4-methoxyphenol was prepared from 1-(2-hydroxy-5-methoxyphenyl)ethan-1-one and ethylmagnesium chloride as colorless oil in 68% yield for two steps.

2.3.2. 2-(*sec*-butyl)-4-methoxyphenyl 4-methylbenzenesulfonate

To a solution of 2-(*sec*-butyl)-4-methoxyphenol (1.0 mmol) in methylene chloride (DCM, 10 mL) was added tosyl chloride (1.1 mmol) and Et₃N (1.1 mmol). The reaction mixture was stirred at room temperature until completion, and water (20 mL) was added into the mixture. The aqueous layer was extracted with DCM. The combined organic layers were washed with brine, dried over anhydrous Na₂SO₄, filtered, and concentrated in vacuo. The residue was purified by flash chromatography to give 2-(*sec*-butyl)-4-methoxyphenyl 4-methylbenzenesulfonate as light-yellow oil in 95% yield.

2.3.3. 2-(*sec*-butyl)-5-chloro-4-methoxyphenyl 4-methylbenzenesulfonate

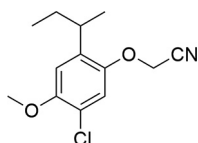
To a solution of 2-(*sec*-butyl)-4-methoxyphenyl 4-methylbenzenesulfonate (1.0 mmol) in glacial acetic acid (5 mL) was added N-Chlorosuccinimide (NCS, 1.2 mmol). The reaction mixture was stirred at room temperature until completion, and saturated NaHCO₃ solution was added into the mixture. The aqueous layer was extracted with ethyl acetate (EtOAc). The combined organic layers were washed with brine, dried over anhydrous Na₂SO₄, filtered, and concentrated in vacuo. The residue was purified by flash chromatography to give 2-(*sec*-butyl)-5-chloro-4-methoxyphenyl 4-methylbenzenesulfonate as a white solid in 72% yield.

2.3.4. 2-(*sec*-butyl)-5-chloro-4-methoxyphenol

To a solution of 2-(*sec*-butyl)-5-chloro-4-methoxyphenyl 4-methylbenzenesulfonate (1.0 mmol) in EtOH (10 mL) was added 2 M NaOH (5 mL). The reaction mixture was stirred at 80 °C until completion, and water (30 mL) was added into the mixture. The

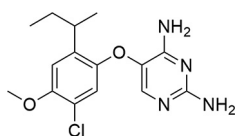
aqueous layer was extracted with EtOAc. The combined organic layers were washed with brine, dried over anhydrous Na₂SO₄, filtered, and concentrated in vacuo. The residue was purified by flash chromatography to give 2-(*sec*-butyl)-5-chloro-4-methoxyphenol as a white solid in 90% yield.

2.3.5. 2-(2-(*sec*-butyl)-5-chloro-4-methoxyphenoxy)acetonitrile



Following the prepare procedure of 2-(2-(*sec*-butyl)-5-chloro-4-methoxyphenoxy)acetonitrile described in our previous work [42], 2-(2-(*sec*-butyl)-5-chloro-4-methoxyphenoxy)acetonitrile was prepared from 2-(*sec*-butyl)-5-chloro-4-methoxyphenol as colorless oil in 72% yield.

2.3.6. 5-(2-(*sec*-butyl)-5-chloro-4-methoxyphenoxy)pyrimidine-2,4-diamine (AF-219-2)



Following the prepare procedure of 5-(2-(*sec*-butyl)-5-chloro-4-methoxyphenoxy)pyrimidine-2,4-diamine described in our previous work [42], 5-(2-(*sec*-butyl)-5-chloro-4-methoxyphenoxy)pyrimidine-2,4-diamine was prepared from 2-(2-(*sec*-butyl)-5-chloro-4-methoxyphenoxy)acetonitrile as a white solid in 65% yield. ¹H NMR (300 MHz, DMSO *d*₆) δ 7.27 (s, 1H), 6.95 (s, 1H), 6.63 (s, 1H), 6.30 (s, 2H), 5.80 (s, 2H), 3.80 (s, 3H), 3.04 (dd, *J* = 14.1, 7.0 Hz, 1H), 1.70–1.42 (m, 2H), 1.18 (d, *J* = 6.9 Hz, 3H), 0.80 (t, *J* = 7.3 Hz, 3H) (Fig. S2). ESI MS *m/z* = 323.1 [M+H]⁺.

2.4. Molecular dynamics (MD) simulations

The homology models of rP2X2^{WT}, rP2X3^{WT} and rP2X2^{gain} were constructed based on the crystal structures of hP2X3 (PDB IDs: 5SVJ and 5YVE) using MODELLER [48]. The alignments of the target sequences were made by ClustalW2 and manually adjusted to match published alignments [49]. The obtained model was checked and validated by ProCheck [50]. The energy-minimized structures of P2X were used as the initial structures for molecular simulations. A large 1-palmitoyl-2-oleoyl-*sn*-glycero-3-phosphocholine (POPC, 300 K) bilayer, available in System Builder of DESMOND [51], was built to generate a suitable membrane system based on the OPM database (<https://opm.phar.umich.edu>) [52], in which the TM domain of the P2X could be embedded properly. The P2X/POPC system was dissolved in simple point charge (SPC) water molecules. Counter ions were then added to compensate for the net negative charge of the system. NaCl (150 mM) was added into the simulation box that represents background salt at physiological condition. The DESMOND default relaxation protocol was applied to each system prior to the simulation run. (1) 100 ps simulations in the NVT (constant number (N), volume (V), and

temperature (T)) ensemble with Brownian kinetics using a temperature of 10 K with solute heavy atoms constrained; (2) 12 ps simulations in the NVT ensemble using a Berendsen thermostat with a temperature of 10 K and small-time steps with solute heavy atoms constrained; (3) 12 ps simulations in the NPT (constant number (N), pressure (P), and temperature (T)) ensemble using a Berendsen thermostat and barostat for 12 ps simulations at 10 K and 1 atm, with solute heavy atoms constrained; (4) 12 ps simulations in the NPT ensemble using a Berendsen thermostat and barostat at 300 K and 1 atm with solute heavy atoms constrained; (5) 24 ps simulations in the NPT ensemble using a Berendsen thermostat and barostat at 300 K and 1 atm without constraint. After equilibration, the MD simulations were performed for ~100–200 ns. Long-range electrostatic interactions were computed using a smooth Particle Mesh Ewald method. The trajectory recording interval was set to 200 ps and other default parameters of DESMOND were used during MD simulation runs. All simulations used the all-atom OPLS_2005 force field [53,54], which was used for proteins, ions, lipids and the SPC waters. All systems were close to overall stability after simulation (Fig. S1). The Simulation Interaction Diagram (SID) module in DESMOND was used for exploring the interaction analysis between AF-219 and P2X. All simulations were run on DELL T7920 graphic working station (with NVIDIA Tesla K40C-GPU). Preparation, analysis, and visualization were performed on a 12-CPU CORE DELL T3610 graphic working station. The protein pockets are detected using Fpocket (<https://fpocket.sourceforge.net/>) [55] and the volume of the cavity is calculated on the TRAPP web server (<https://trapp.h-its.org/trapp>) [56].

2.5. Data analysis

All results are expressed as Mean ± S.E.M. or S.D., and statistics are analyzed using Student's *t* test or ANOVA, for which **P* < 0.05 and ***P* < 0.01 were considered as significant difference. Concentration-response curves were fitted to the Hill equation: $I/I_{max} = 1/(1+(IC_{50}/[inhibitor])^n)$, in which *I* is the normalized current at a given of the concentration of the antagonists, *I*_{max} is the maximum normalized current induced by the agonist (ATP), [*inhibitor*] is the concentration of AF-219, AF-353, and synthesized analogs of AF-353, *IC*₅₀ is the antagonist concentration that is half maximally effective, *n* is the Hill coefficient.

3. Results

3.1. The negative allosteric site of AF-219 on the P2X3 receptor is also present in other subtypes, but the accessibility of the small molecule differs from that of P2X3

We previously found that the relative motion of the LF and dorsal fin (DF) domains of P2X4 receptors is critical for the transition of the channel from the resting state to the open state [44]. Comparison of the resolved structures of hP2X3 [57] and rP2X7 [58] in the open state with those in the *apo* state revealed that relative movements of the LF and DF domains also occur in other P2X subtypes, indicating that, in addition to P2X4, this allostery may play an important role in other subtypes of channel gating. In a recent study, we also found that the P2X3 receptor antagonist AF-219 and its derivatives AF-353 and RO-51 bind within the allosteric site formed by the LF and lower body (LB) domains and exert an inhibitory effect by impeding the relative movement of the LF and DF domains during P2X3 opening (Fig. 1A and Ref. [42]). Whether this negative allosteric pocket exists only at the P2X3 receptors or whether there are other possibilities is not well understood.

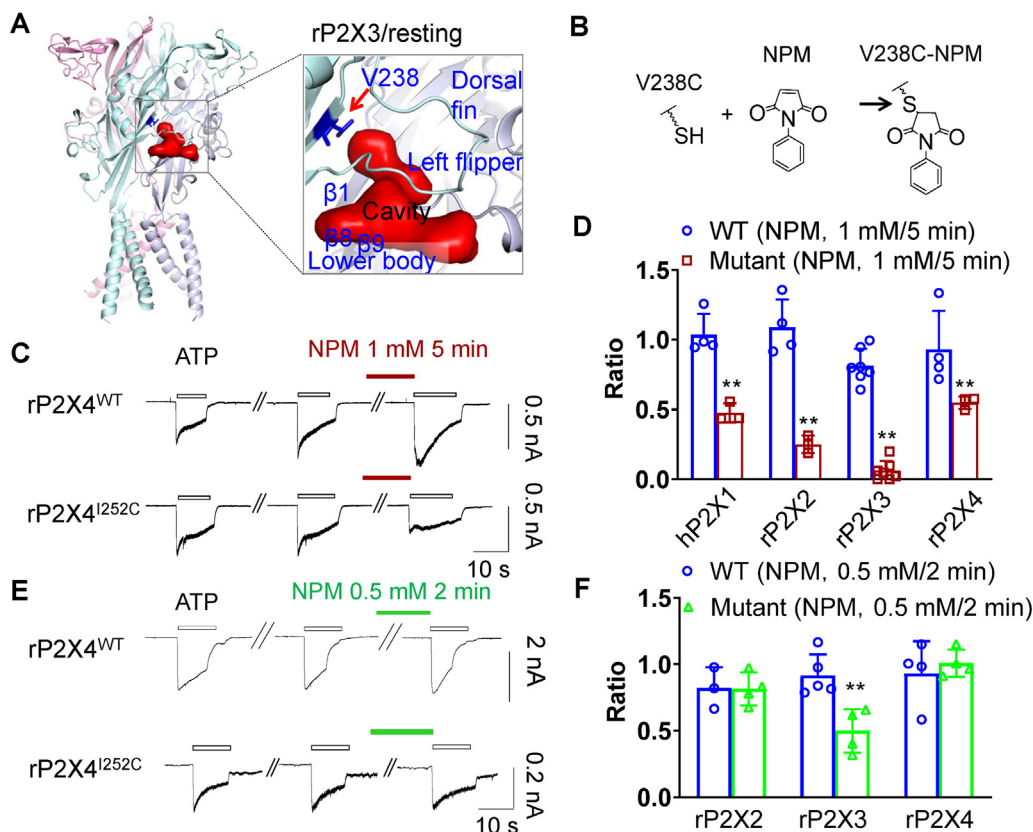


Fig. 1. Covalently linking the NPM to residue 238 substituted by cysteine in rP2X3 and to the identical position in other P2X subtypes. (A) View of the pocket formed by the left flipper (LF) and lower body (LB) domains of rP2X3. (B) Illustration of NPM covalently linked to rP2X3^{V238C}. Equivalent position mutations in hP2X1, rP2X2, rP2X4 and rP2X7 are V252C, V249C, I252C and I251C, respectively. (C–D) Representative current traces (C) and pooled data (D, mean \pm S.D., $n = 3-7$) show the effect of NPM (1 mM, 5 min) on the wild type (WT) and equivalent cysteine substitutions in P2X receptors. ATP concentrations of 10 μ M, 100 μ M, 10 μ M, and 100 μ M and 1 mM were applied in hP2X1, rP2X2, rP2X3, and rP2X4, respectively. * $P < 0.01$ versus WT, two-way ANOVA with *Bonferroni post-hoc* test. (E–F) Representative current traces (E) and pooled data (F, mean \pm S.D., $n = 3-5$) show the effect of NPM (0.5 mM, 2 min) on wild type (WT) and equivalent cysteine substitutions in P2X receptors. ** $P < 0.01$ versus WT, two-way ANOVA with *Bonferroni post-hoc* test.

To address this question, we covalently linked small molecules to specific amino acids of each subtype, corresponding to cysteine mutation inside the AF-219 binding pocket, like V238C in rP2X3, to verify whether the opening of the other P2X subtypes would be affected if the relative movement of the LF and DF domains was blocked. We constructed mutants hP2X1^{V252C}, rP2X2^{V249C}, rP2X3^{V238C}, rP2X4^{I252C} and rP2X7^{I251C} at equal positions in five different subtypes (P2X5 and P2X6 receptors were not measured due to their ATP responses are almost undetectable), and then reacted with the introduced free thiol group (-SH) (Fig. 1B) using 1 mM N-phenylmaleimide (NPM) with 5 min pretreatment to achieve covalent occupation of the small molecule at this position. Compared with wild type (WT) P2X receptors, hP2X1^{V252C}, rP2X2^{V249C}, rP2X3^{V238C} and rP2X4^{I252C} have significantly impaired channel functions after forming a covalent linkage with NPM (Fig. 1C, D), indicating that the allosteric pocket recognizing AF-219/AF-353/RO-51 not only has the potential to allosterically regulate P2X3 receptors but also the other subtypes of P2X receptors are also prevalent, at least for hP2X1, rP2X2 and rP2X4. NPM modification of the rP2X7^{I251C} receptor was not carried out, as its ATP response was almost undetectable (Fig. S3).

When the concentration of NPM was reduced to 0.5 mM and the reaction time to 2 min, there was still a significant decrease in the ATP current rP2X3^{V238C}, while rP2X4^{I252C} and rP2X2^{V249C} showed no significant change (Fig. 1E, F), indicating that the accessibility of small molecules to this pocket was different among different subtypes.

3.2. Amino acid sequence differences at the entrance affect the small molecule accessibility to the negative allosteric site

To further confirm this point, we examined the cavity between the LF and LB domains in the structures of rP2X3 and zebra fish P2X4 (zFP2X4) (Fig. 2A, B). Consistent with above covalent modification results, a pocket consisting of amino acids in $\beta 1$, $\beta 8$ and $\beta 9$ sheets of the LB and LF domains is present below the LF domain of both zFP2X4 and rP2X3 receptors. The difference is that in rP2X3, the entrance of the pocket is the glycine (G189), a residue without a bulky side chain, so that the pocket is accessible (Fig. 2A). However, in zFP2X4, the corresponding residue is an arginine (R203), whose bulkier side chain making the pocket inaccessible to small molecules (Fig. 2B).

Since any mutation of R203 in the rP2X4 or zFP2X4 receptors abolishes the activation of channels [59], it is difficult to verify the effect of reducing the side chain size of the entrance of putative allosteric site at the P2X4 receptor. However, by analyzing the sequences of P2X3 receptors of other species, it was found that in the chicken P2X3 (cP2X3) receptor, the identical position is an alanine (Fig. 2C), providing a good tool to study the accessibility of the AF-219 pocket in P2X3. Furthermore, AF-353, which has only one sulfonamide group substituted by an iodine atom, has a higher affinity (~ 10 -fold) and stable inhibition of the P2X3 receptor compared with AF-219; our previous results also showed that AF-353 and other analogs do act in the same pocket formed by the LF and LB domains [42]. Therefore, we used AF-353 as a chemical tool

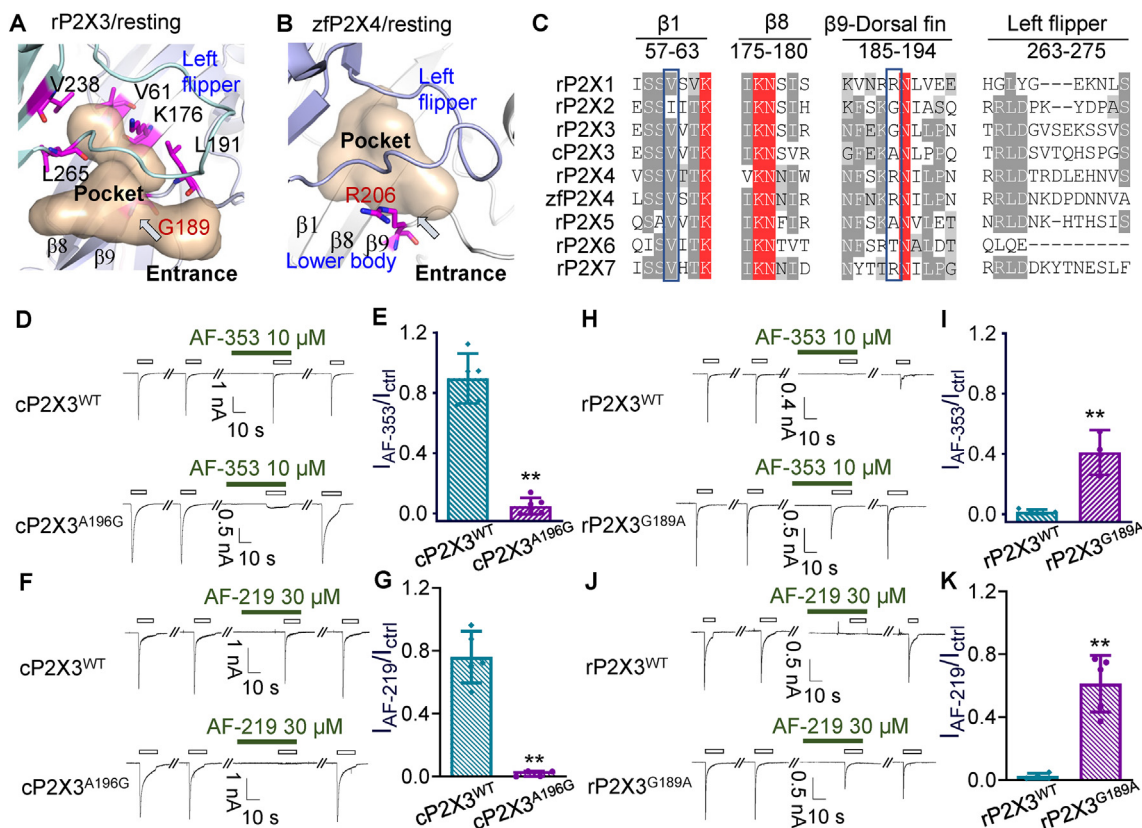


Fig. 2. G189 determines the accessibility of small molecules to the negative allosteric site formed by the left flipper (LF) and lower body (LB) domains of the pocket fostered by the LF and LB domains of P2X3. Residues forming this pocket are indicated by sticks for emphasis. (A) Zoom-in view of the pocket fostered by the LF and LB domains of the equivalent pocket in the zfP2X4 receptor. The bulky side chain of R206 (shown on sticks for emphasis) blocks the entrance to this pocket. (B) Zoom-in view of the equivalent pocket in the zfP2X4 receptor. (C) Amino acid sequence alignment of residues constituting the proposed site in different P2X receptors. (D–G) Typical current traces (D, F) and pooled data (E, G) showing the effect of AF-353 (D, E, 10 μM) and AF-219 (F, G, 30 μM) on the ATP (10 μM)-current of cP2X3^{WT} and cP2X3^{A196G}. Data are expressed as mean ± S.D. (n = 4–6). **P < 0.01 compared to WT, Student's *t*-test. (H–K) Typical current traces (H, J) and pooled data (I, K) showing the effect of AF-353 (H, I, 10 μM) and AF-219 (J, K 30 μM) on the ATP (10 μM)-current of rP2X3^{WT} and rP2X3^{G189A}. Data are expressed as mean ± S.D. (n = 3–5). **P < 0.01 compared to WT, Student's *t*-test.

in all subsequent functional analyses, and key findings were simultaneously validated with AF-219.

Consistent with our inference, since the amino acid corresponding to G189 of rP2X3 is alanine (A196 in cP2X3), 10 μM of AF-353 and 30 μM of AF-219 had no inhibitory effect on cP2X3 at all (Fig. 2D–G). Also, G189A mutation in rP2X3 abolished the inhibition of AF-353 and AF-219 (Fig. 2H–K). Notably, after mutating this site to glycine, cP2X3^{A196G} then gained the ability to be significantly inhibited by AF-353/AF-219 (Fig. 2D–G), demonstrating the importance of the G189 position for small molecules to enter and act in the pocket below the LF domain. This also appears to be consistent with the finding that treatment with 0.5 mM/2 min NPM could modify rP2X3^{V238C}, since the position corresponding to G189 is glycine, but not in rP2X4^{I252C} where G189 corresponds to arginine (Fig. 1E, F).

3.3. Sequence changes in residues located deep in the allosteric pocket may prevent small molecules from binding deeper into the pocket

The difference in amino acid sequence at the entrance could explain the insensitivity of AF-219 to a few subtypes like P2X4 that have a bulkier side chain of amino acids at the entrance. In contrast, rP2X2 contains the same glycine at position 201 (Fig. 2C and 3A), suggesting that the difference in amino acids at the entrance is not sufficient to fully explain the high selectivity of AF-219. To further illustrate this, we constructed a homology model of AF-219 in complex with rP2X2 (Fig. 3A).

The initial structure of the homology modeling suggests that in P2X2, AF-219 took a similar interaction as P2X3 (Fig. 3B). Further,

we took ~200-ns time scale of MD simulations to investigate whether this interaction is stable. In the P2X3 receptor, the hydrophobic interaction of V61 with AF-219 is important for AF-219 binding, and mutation of V61R leads to a significant decrease in AF-219 affinity [42]. In P2X2, the amino acid in the identical position is I67, and this position is the only amino acid that differs in the direct interaction of AF-219 with rP2X2 or rP2X3 (Fig. 3B). To illustrate whether the binding of AF-219 is stable, we monitored the change in the distance between the C_α atom of I67 and the O atom of AF-219 during MD simulations (Fig. 3C), and we found that this distance changed significantly from 8.5 to ~12 Å during simulations, suggesting that AF-219 is ‘forced’ to move out during MD simulations (Fig. 3C–E) due to the larger steric hindrance of Ile (I67 in rP2X2) than Val (V67 in rP2X3).

In fact, P2X2^{I67V} partially obtained the inhibition of AF-353 compared to the WT P2X2 channel (with a maximum inhibition of ATP currents at 100 μM (maximal water solubility) = 67.8 ± 5.3%, IC₅₀ > 10 μM; Fig. 3F), a result suggesting that the binding and action of the small molecule antagonist require access to the deeper region of this allosteric pocket, and V61 contributes to the binding of small molecules entering the deeper region of the pocket.

3.4. The difference in pocket shape is another important factor in determining the role of small molecules

Although rP2X2^{I67V} ‘gains’ AF-353-sensitivity, the IC₅₀ value of AF-353 for rP2X2^{I67V} differs nearly 1000-fold from that of rP2X3, suggesting that there are factors other than pocket accessibility

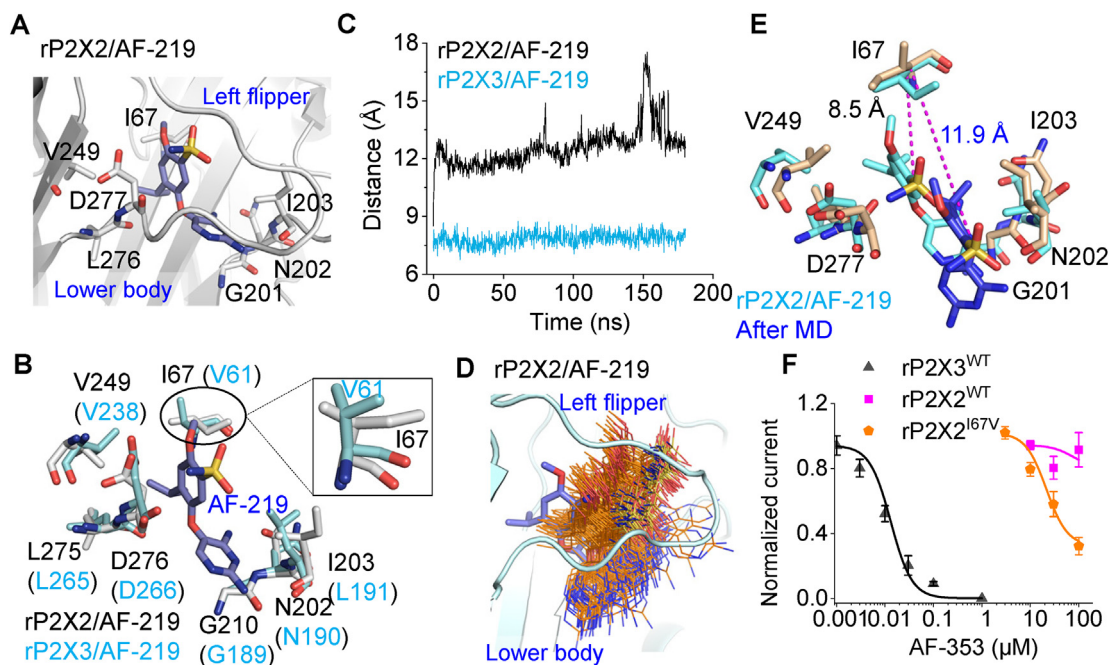


Fig. 3. V61 contributes to the binding of small molecules to the deeper region of the pocket. (A) Zoom-in view of interaction between rP2X2 and AF-219 in homology model of the rP2X2/AF-219 complex. (B) Superposition of key residues of rP2X2 (gray) and hP2X3 (cyan) in contact with AF-219. I67 in P2X2 and V61 in P2X3 were zoomed in to show clearly. (C) Distance between the O atom of AF-219 and the C α of I67 in rP2X2 (black) or V61 in rP2X3 (cyan) measured over time in 180-ns MD simulations. (D) Superposition of all poses of AF-219 during the 180-ns MD simulation. The initial pose of AF-219 is indicated by blue sticks and the poses during the MD simulation by origin lines. (E) Superposition of the initial (wheat) and optimized poses (blue) after MD simulation of the rP2X2 model in complex with the AF-219. The magenta dashed line indicates the distance between AF-219 and V61. (F) Concentration-response curves for AF-353 for rP2X3^{WT}, rP2X2^{WT} and rP2X2^{I67V} (n = 3–6).

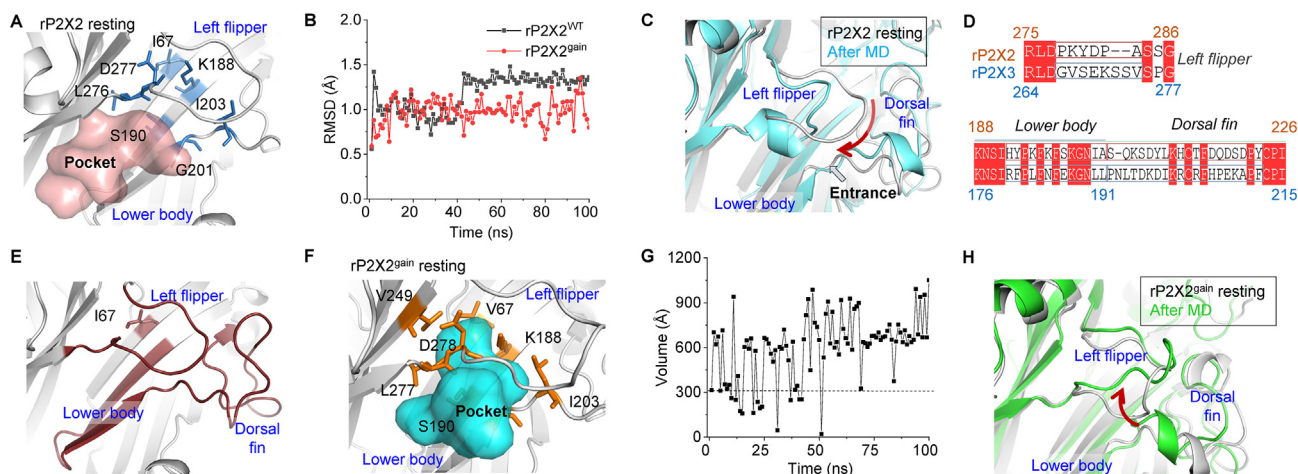


Fig. 4. Dynamics of the allosteric site formed by the LF and LB domains. (A) Zoom-view of the pocket fostered by the LF and LB domains of rP2X2. Residues forming this pocket are indicated by sticks for emphasis. (B) Measured RMSD of C α atoms of amino acids that constitute the pocket during MD simulations for rP2X2^{WT} and rP2X2^{gain} over time in 100-ns MD simulations. (C) Comparison of the initial structure (gray) and the snapshot (cyan) after 100 ns of simulation on rP2X2^{WT}. The red arrow indicates the movement of the LF domain during simulations. (D) Amino acid sequence alignment of the LF, DF and LB structural domains between rP2X2 and rP2X3. (E) The region of rP2X2 (including residues 67, 188–226, and 275–286, brown) is substituted by the corresponding residues of rP2X3. (F) Zoomed-in view of the pocket fostered by the LF and LB domains of rP2X2^{gain} in the resting state. (G) Volume measurements during MD simulation for rP2X2^{gain}. (H) Comparison of the initial structure (gray) and a snapshot (green) after 100-ns MD simulation on rP2X2^{gain}. The red arrow indicates the motion of the LF domain.

and deep pocket size that influence AF-219/AF-353 binding. Because of the sequence differences in the amino acids that make up this pocket, we used Fpocket (<https://fpocket.sourceforge.net/>) [59] to characterize this pocket of the rP2X2 receptor and found that in the resting state of rP2X2, this pocket is closer to the surface of the protein compared to rP2X3 (Fig. 4A). Furthermore, the root-mean-square deviation (RMSD) analysis of the amino acids constituting this pocket changed from 1 Å in the initial step to ~1.5 Å at the final snapshot of MD simulations

(Fig. 4B), indicating that sequence differences may lead to significant structural rearrangements in this region. Interestingly, after MD simulations, the LF domain shifted downward to form an α -helical structure, and such a change resulted in a compressed pocket below the LF domain, thus making AF-219 difficult to access (Fig. 4C). This is consistent with the finding that treatment with 0.5 mM/2 min NPM had no effect on rP2X2^{V252C} (Fig. 1F), although the position corresponding to P2X3-G189 in rP2X2 is also glycine (G201, Fig. 4A, C).

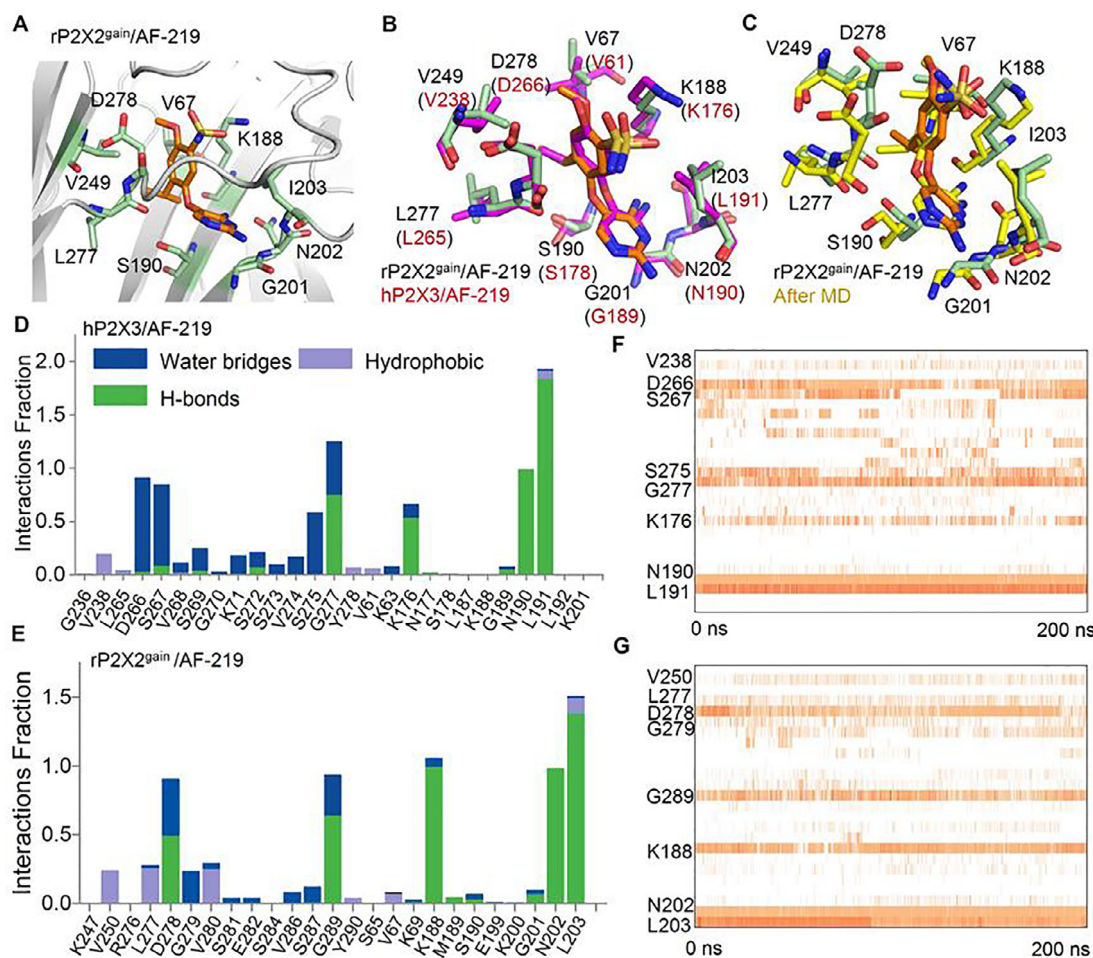


Fig. 5. MD simulations reveal the interaction of rP2X2^{gain} with AF-219 at atomic level. (A) Homology model of rP2X2^{gain} in complex with AF-219. (B) Superposition of key residues of rP2X2^{gain} (cyan) and hP2X3 (salmon) interacting with AF-219. (C) The superposition of the initial (cyan) and MD-optimized (yellow) poses of rP2X2^{gain} in complex with AF-219. (D-E) P2X-ligand contacts of hP2X3 (D) and rP2X2^{gain} (E) with the AF-219 were monitored throughout the MD simulations. P2X-ligand contacts were categorized into three types: hydrogen Bonds (green), hydrophobic (light blue), and water bridges (blue). The stacked bar charts were normalized over the course of the trajectory (values over 1.0 are possible as some protein residue may make multiple contacts of the same subtype with the ligand). (F-G) Timeline representation of the interactions and contacts between hP2X3 (F) and rP2X2^{gain} (G) with AF-219 monitored throughout the MD simulations (some residues made more than one specific contact with the ligand were represented by a darker shade of orange). Only the binding site residues interacting with the ligand are marked with numbers.

We constructed a chimera homology model in which the corresponding regions of P2X2 that constitute the pocket, including the LF and LB domains, were replaced with identical sequences of P2X3 (Fig. 4D) and added a substitution of I67V to obtain a new chimera P2X2^{gain} (Fig. 4E, F). Analysis of the pocket properties of this chimera by TRAPP web server (<https://trapp.h-its.org/trapp>) [56] revealed that the heterologous pocket became larger rather than smaller after MD simulations, a result of upward motion of LF domain (Fig. 4F-H) during simulations. These results suggested that sequence variants of the LF, LB and DF domains could influence the shape of this site.

In the simulation system, we further integrated AF-219 into the P2X2^{gain} model (Fig. 5A), where the binding pattern of AF-219 remained consistent with the crystal structure of the hP2X3/AF-219 complex (Fig. 5B). On this basis, MD simulations of the AF-219/P2X2^{gain} complex showed that the contact of AF-219 with P2X2^{gain} did not change significantly before and after MD simulations (Fig. 5C), unlike its extrusion from the pocket in the P2X2 WT channels (Fig. 3C-E). hP2X3 (Fig. 5D) and rP2X2^{gain} (Fig. 5E) interactions with the AF-219 were monitored throughout the MD simulations. These interactions were categorized by type and summarized into three types: hydrogen bonds, hydrophobic, and water bridges, and the stacked bar charts were normalized over the

course of the trajectory (for example, a value of 0.5 suggests that 50% of the simulation time the specific interaction is maintained; values over 1.0 are possible as some residues may make multiple contacts of the same subtype with the ligand). The timeline representation of the interactions and contacts were also summarized in the Fig. 5F, G (some residues made more than one specific contact with the ligand were represented by a darker shade of orange). These analyses indicated that AF-219 had interactions with V250, L277, D278, G279, G289, K188, N202 and L203 of P2X2^{gain} (corresponding to V238, D266, S267, S275, G277, K176, N190 and L191 of P2X3), which is essentially comparable to interactions of AF-219 and hP2X3 that observed in the crystal structure (Fig. 5D, E).

To verify this point, the chimeras rP2X2^{LF}, rP2X2^{LBD/DF}, rP2X2^{LF/LBD/DF} and rP2X2^{gain} were obtained by stepwise substitution of the amino acids constituting the rP2X2 binding pocket (Fig. 6A). rP2X2^{LBD/DF} substitution only mildly enhanced the antagonistic effect of AF-353 (IC₅₀ > 100 μM), whereas in the case of both substitutions, i.e., rP2X2^{LF/LBD/DF} significantly enhanced the antagonistic effect of AF-353 (IC₅₀ = 10.7 ± 3.2 μM). If rP2X2^{I67V} was incorporated into rP2X2^{LF/LBD/DF}, namely P2X2^{gain}, the antagonistic effect of AF-353 can be increased ~20-fold (IC₅₀ = 0.33 ± 0.02 μM, Fig. 6B).

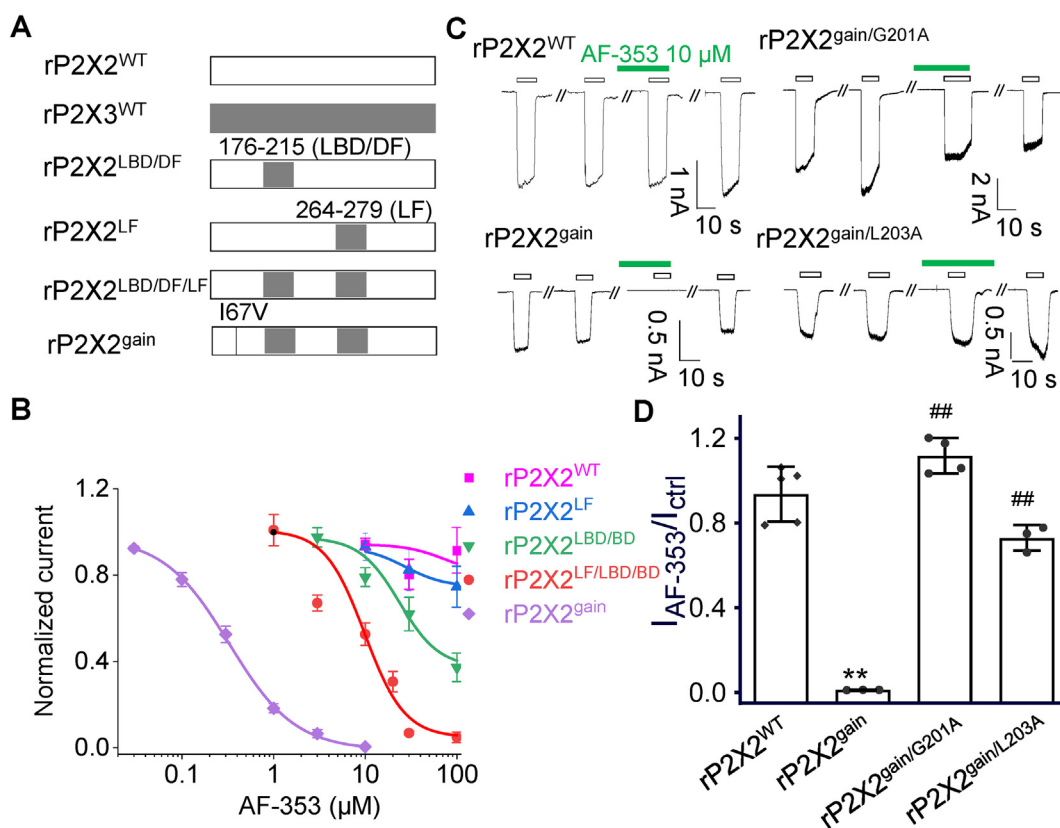


Fig. 6. Combination of factors producing subtype selectivity of AF-353/AF-219 generates the AF-353/AF-219-sensitive chimera P2X2^{gain}. (A) Schematic representation of chimera construction. rP2X2 chimeras were generated by replacing certain regions of rP2X2 with the corresponding sequences of rP2X3. (B) Concentration response curves of AF-353 in different chimeras (mean ± SEM, n = 3–5). (C–D) Representative currents (C) and pooled data (D) of ATP (10 μM) induced currents of AF-353 (10 μM) on rP2X2 WT and mutants (mean ± S.D., n = 3–5). **P < 0.01 versus rP2X2^{WT}, ##P < 0.01 versus rP2X2^{gain}, one ANOVA with Bonferroni post-hoc test.

In addition, further mutations based on rP2X2^{gain}, rP2X2^{gain}-G201A (corresponding to G189 of rP2X3) or rP2X2^{gain}-L203A (a residue corresponding to L191 of rP2X3, whose backbone atom forms hydrogen bonding interaction with AF-219; rP2X3^{L191A} almost fully abolished the inhibition of AF-353 and AF-219 [42]), greatly weakened the antagonistic effect of AF-353 in rP2X2^{gain} (Fig. 6C, D). These results again validate the important influence of G201 as a key residue at the entrance of the pocket and suggest that the protein–ligand interaction of rP2X2^{gain}/AF-353 is similar to that exhibited in the P2X3/AF-219 crystal structure.

3.5. In addition to the binding site amino acids directly contacting with AF-353/AF-219, other amino acids also have an impact on ligand recognition

Although we replaced almost all amino acids around the AF-219 binding site in rP2X2, rP2X2^{gain} and rP2X3^{WT} still differ ~20–50-fold in IC₅₀ values of AF-353 and AF-219, suggesting that structural elements outside the allosteric site also have an effect on the binding and action of these allosteric modulators. Sequence differences in the non-binding site may lead to slight differences in the properties of the allosteric site. To test this idea, we synthesized AF-219-1 and AF-219-2, two compounds that differ slightly from the AF-219 and AF-353 (Fig. 7A). If the pockets of rP2X2^{gain} and rP2X3^{WT} maintained exactly the same conformation, the different AF-219/AF-353 analogs would exhibit the same alteration in the concentration response curves of P2X2^{gain} versus rP2X3^{WT}. We measured the IC₅₀ values of four compounds, AF-353, AF-219, AF-219-1 and AF-219-2, on rP2X3^{WT} and rP2X2^{gain}, respectively (Fig. 7B, C). The IC₅₀ values for all four antagonists were greater

for rP2X2^{gain} than for rP2X3^{WT}, with a 33-fold increase for AF-353, a 92-fold increase for AF-219, a 30-fold increase for AF-219-1, and an 18-fold increase for AF-219-2, indicating different alterations in the concentration response curves of P2X2^{gain} versus rP2X3^{WT}. Under the condition that the amino acids forming the allosteric pocket of P2X2^{gain} and rP2X3^{WT} are nearly identical, these differences may be caused by the different amino acid residues outside the pocket.

4. Discussion

P2X receptors are currently gaining attention as an important new class of drug targets [60]. The crystal structures of several subtypes have been determined, and drug discovery of P2X receptors is no longer limited to the traditional high-throughput screening. New drug development and chemical structure optimization by means of computer-aided design or artificial intelligence approaches will be another important strategy [42,61]. The success of AF-219 in phase III clinical trials has prompted us to extensively investigate its mechanism of action [9,62,63]. Although we have identified the site of action of AF-219 previously [42], the development of new drugs at this site still requires our understanding of the mechanism by which AF-219 selectively acts at the P2X3 receptor.

In the crystal structure of P2X3 complexed with AF-219, the small molecule is bound in a pocket consisting of the LF and LB domains and forms hydrogen bonding interactions with main chain atoms of N190/L191 [42]. From the results of NPM modification, this pocket is also present in P2X1, P2X2, and P2X4, and some amino acids interacting with AF-219, such as N190, V238 and

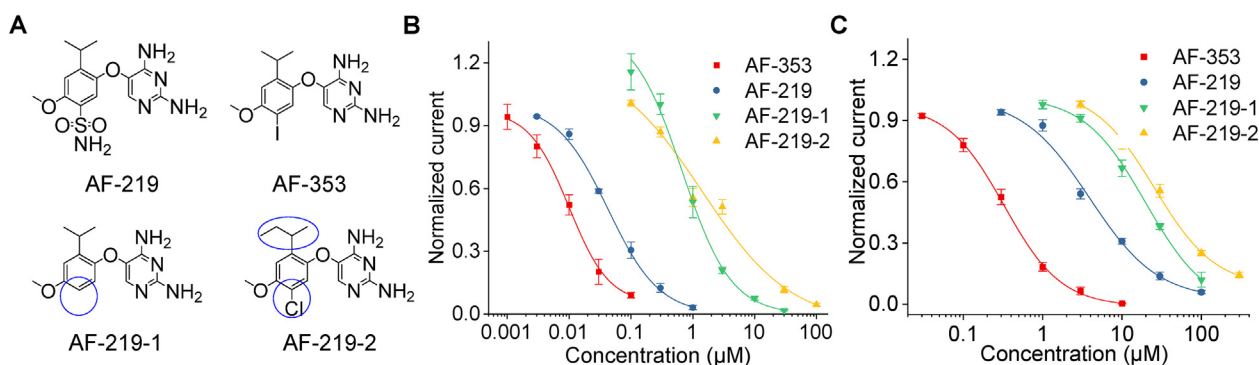


Fig. 7. Effect of AF-219 derivatives on the ATP current of rP2X3^{WT} and rP2X2^{gain}. (A) Chemical structures of various AF-219 derivatives. (B–C) Concentration response curves of AF-219, AF-353, AF-219-1 and AF-219-2 to rP2X3^{WT} (B) and rP2X2^{gain} (C). The data of AF-353 are the same as shown in Figs. 3F and 6B and are shown here for comparison. The data are shown as mean \pm SEM ($n = 3$ –6).

D266, are highly conserved in different subtypes of P2X. Although some amino acids such as L191 have isoleucine replacement in other subtypes, AF-219 interacts only with the backbone atoms at that position. Thus, each P2X receptor subtype has its own specificity of allosteric sites [64], and the selective action of AF-219 on the P2X3 receptor is determined not only by differences in the amino acid sequences with which it interacts directly, but also by amino acids outside the pocket.

The accessibility of the binding pocket affects the action of AF-219 in two ways. *First*, the amino acid at the entrance of the pocket is glycine in rP2X3, ensuring that AF-219 enters this pocket smoothly. Any small change including G189A causes a dramatic change in the inhibitory effect of AF-219 [42]. Since there is no significant change in the activation of P2X3^{G189A} by ATP, it is less likely that the pocket conformational change caused by the alanine substitution affects the inhibitory effect of AF-219, though we cannot completely rule out this possibility. The ability of the A196G substitution in chicken P2X3 to change the genus P2X3 from AF-353 insensitive to sensitive is also evidence for this view. In addition to the role of steric hindrance, other subtypes of arginine at this position may also affect AF-219 binding through additional contacts with neighboring residues [65]. *Second*, the size of the amino acid side chain within the pocket determines whether AF-219 binds stably. The hydrophobic interaction of V61 with AF-219 in P2X3 is important for maintaining AF-219 [42], and changing the amino acid side chain at position 61 would result in AF-219 not binding stably at the position where it should. Therefore, reducing the side chain of isoleucine at this position to Val in the P2X2 receptor partially restores its AF-353 sensitivity.

In addition, differences in the overall architecture or amino acids outside the binding pocket of P2X receptors of different species and subtypes can also have an impact on the binding of small molecules, especially for ligands that bind to the same pocket with subtle conformational differences. This may seem difficult to understand, but it reflects the flexibility of the channel proteins themselves that underlie remote allosteric regulation [66]. Some amino acid residues that appear to be far from the allosteric site can also affect the conformation of these sites; after all, the protein functions as a unity. Just as the binding of small molecules beneath the LF domain can affect the activation of P2X by ATP, sequence differences outside the binding pocket can also significantly affect allosteric regulation, as is the case with the inhibitory effect of the hP2X3-A197/T201 mutation on RO-51 (these two positions are far from the identified allosteric site) [67].

Finally, although various P2X subtypes are highly conserved and the allosteric site of AF-219/AF-353 may also be present on the other subtypes of P2X receptors, the binding and interaction of small molecule ligands with the binding site require a high

degree of substitution of water molecules in the binding pocket [68], as well as a high degree of fitting of entropy and enthalpy changes [69], and even the influence of amino acids outside the binding pocket on the overall conformation of the binding pocket. Additionally, various subtypes of the P2X receptor and different species differ in their amino acid sequences at several amino acids in direct contact with AF-219/AF-353, and there are also significant differences in amino acid sequences between the LF, DF, LBD, and adjacent head domains of the different subtypes comprising this allosteric pocket (especially the LF and head domains), making it difficult to meet the conditions for high-affinity binding of small molecules [66,70], leaving open the possibility of finding subtype-selective antagonists, such as AF-353 and AF-219, as well as drug optimization and new drug development based on them.

5. Conclusion

Although we previously identified the site and mechanism of action of AF-219 on the P2X3 receptor, which occupies a pocket consisting of the left flipper and lower body (LB) domains, the mechanism by which Gefapixant/AF-219 selectively acts on the P2X3 receptor is unclear. We suggest here that the negative allosteric site of AF-219 at P2X3 is also present in other P2X subtypes and the selectivity of AF-219 or AF-353 for P2X3 over other P2X subtypes is determined by the accessibility of its binding site and the shape constraints of its pocket, a finding that will provide new perspectives for drug design against P2X3-mediated diseases such as RCC, idiopathic pulmonary fibrosis and overactive bladder disorder.

Declaration of Competing Interest

The authors declare that they have no known competing financial interests or personal relationships that could have appeared to influence the work reported in this paper.

Acknowledgments

This study was supported with funds from the Natural Science Foundation of Jiangsu Province (BK20202002 to Y. Y.), National Natural Science Foundation of China with grant numbers 32000869 (J. W.), 31900808 (X. -N. Y.), 81902480 (W. -H. W.), 31971146 (Y. Y.) and 32071234 (M.H.), Innovation and Entrepreneurship Talent Program of Jiangsu Province (Y. Y. and J. W.), State Key Laboratory of Utilization of Woody Oil Resource with grant number 2019XK2002 (C. -Z. L.), Hunan “Huxiang” High-level Talent Program (2021 to Y. Y) and “Xing Yao” Leading

Scholars of China Pharmaceutical University (2021 to Y. Y.). This work was also supported by the Innovative Research Team of High-level Local Universities in Shanghai and a key laboratory program of the Education Commission of Shanghai Municipality (ZDSYS14005 to M. H.), and by the Open Research Fund of State Key Laboratory of Genetic Engineering, Fudan University (No. SKLGE-2105 to M. H.) and State Key Laboratory of Drug Research (No. SIMM2105KF-14 to Y. Y.).

Author Contributions

Y Yu initiated the project. Y Yu and J Wang designed research. WW Cui, SY Wang, YQ Zhang, Y Wang, YZ Fan, CR Guo, XH Li, YT Lei, WH Wang, XN Yang, M Hattori, CZ Li, J Wang and Y Yu performed research. WW Cui, SY Wang, J Wang and Y Yu analyzed data. WW Cui, SY Wang, J Wang and Y Yu wrote the manuscript. All authors discussed the results and commented on the manuscript.

Appendix A. Supplementary data

Supplementary data to this article can be found online at <https://doi.org/10.1016/j.csbj.2022.03.030>.

References

- Illes P, Muller CE, Jacobson KA, Grutter T, Nicke A, Fountain SJ, et al. Update of P2X receptor properties and their pharmacology: IUPHAR Review 30. *Br J Pharmacol* 2021;178:489–514.
- Kennedy C. That was then, this is now: the development of our knowledge and understanding of P2 receptor subtypes. *Purinergic Signal* 2021;17:9–23.
- Burnstock G. The therapeutic potential of purinergic signalling. *Biochem Pharmacol* 2018;151:157–65.
- Muccino D, Green S. Update on the clinical development of gefapixant, a P2X3 receptor antagonist for the treatment of refractory chronic cough. *Pulm Pharmacol Ther* 2019;56:75–8.
- Morice AH, Kitt MM, Ford AP, Tershakovec AM, Wu WC, Brindle K, et al. The effect of gefapixant, a P2X3 antagonist, on cough reflex sensitivity: a randomised placebo-controlled study. *Eur Respir J* 2019;54.
- Smith JA, Kitt MM, Butera P, Smith SA, Li Y, Xu ZJ, et al. Gefapixant in two randomised dose-escalation studies in chronic cough. *Eur Respir J* 2020;55.
- Smith JA, Kitt MM, Morice AH, Birring SS, McGarvey LP, Sher MR, et al. Gefapixant, a P2X3 receptor antagonist, for the treatment of refractory or unexplained chronic cough: a randomised, double-blind, controlled, parallel-group, phase 2b trial. *Lancet Respir Med* 2020;8:775–85.
- Abu-Zaid A, Aljaili AK, Althaqib A, Adem F, Alhalal DA, Almubarak AF, et al. Safety and efficacy of gefapixant, a novel drug for the treatment of chronic cough: A systematic review and meta-analysis of randomized controlled trials. *Ann Thorac Med* 2021;16:127–40.
- McGarvey LP, Birring SS, Morice AH, Dicipinigaitis PV, Pavord ID, Schelfhout J, et al. Efficacy and safety of gefapixant, a P2X3 receptor antagonist, in refractory chronic cough and unexplained chronic cough (COUGH-1 and COUGH-2): results from two double-blind, randomised, parallel-group, placebo-controlled, phase 3 trials. *Lancet* 2022;399:909–23.
- Morice A, Smith JA, McGarvey L, Birring SS, Parker SM, Turner A, et al. Eliapixant (BAY 1817080), a P2X3 receptor antagonist, in refractory chronic cough: a randomised, placebo-controlled, crossover phase 2a study. *Eur Respir J* 2021.
- Bayer. Clinical study to evaluate the efficacy and safety of three different doses of BAY1817080 compared to placebo in patients with chronic cough. <https://ClinicalTrials.gov/show/NCT04562155>; 2020.
- Bayer. Repeat doses of BAY1902607 in healthy males and proof of concept in chronic cough patients. <https://ClinicalTrials.gov/show/NCT03535168>; 2018.
- Birring SS, Smith JA, Morice AH, Sher M, Hull JH, Goldsobel AB, et al. Improvements in cough severity and cough-related quality of life in a phase 2 trial (RELIEF) with the P2X3 antagonist BLU-5937 in refractory chronic cough (RCC). *Eur Respir J* 2021;58:OA1199.
- Inc BH. Evaluation of the efficacy and safety of BLU-5937 in adults with refractory chronic cough. <https://ClinicalTrials.gov/show/NCT04678206>; 2020.
- Ishihara H, Hida H, Machida M, Tsuda Y, Miyazaki S. Design of phase 2b randomised controlled trial of S-600918, P2X3 receptor antagonist for refractory chronic cough. *Eur Respir J* 2020;56:2271.
- Shionogi, Inc. S. Evaluation of S-600918 in adults with refractory chronic cough. <https://ClinicalTrials.gov/show/NCT04110054>; 2020.
- Bayer. Study to gather information how well three different doses of BAY1817080 Given twice daily over 12 weeks work in comparison to an inactive pill (placebo) and elagolix in women suffering from pain related to a condition where the tissue that usually grows inside the womb grows outside of the womb. <https://ClinicalTrials.gov/show/NCT04614246>; 2021.
- Bayer. Clinical study to evaluate the treatment effect and safety of BAY1817080 in patients with overactive bladder (OAB). <https://ClinicalTrials.gov/show/NCT04545580>; 2020.
- Inoue K. Nociceptive signaling of P2X receptors in chronic pain states. *Purinergic Signal* 2021;17:41–7.
- <https://www.biospace.com/article/nippon-chemiphar-presents-promising-data-on-novel-prescription-cough-medicine-representing-possibly-second-new-rx-cough-drug-to-enter-market-since-1950s/>.
- Stock TC, Bloom BJ, Wei N, Ishaq S, Park W, Wang X, et al. Efficacy and safety of CE-224,535, an antagonist of P2X7 receptor, in treatment of patients with rheumatoid arthritis inadequately controlled by methotrexate. *J Rheumatol* 2012;39:720–7.
- <https://adisinsight.springer.com/drugs/800025672>.
- Kim JY, Lee EJ, Seong YJ, Ahn Y, Park S, Lee J, et al. AZD-9056, a P2X7 receptor inhibitor, suppresses ATP-induced melanogenesis. *J Dermatol Sci* 2020;100:227–9.
- AstraZeneca. A 6-month randomised, double-blind, open arm comparator, phase IIb, with AZD9056, in patients with rheumatoid arthritis (RA). <https://ClinicalTrials.gov/show/NCT00520572>; 2007.
- Ali Z, Laurijssens B, Ostenfeld T, McHugh S, Stylianou A, Scott-Stevens P, et al. Pharmacokinetic and pharmacodynamic profiling of a P2X7 receptor allosteric modulator GSK1482160 in healthy human subjects. *Br J Clin Pharmacol* 2013;75:197–207.
- Territo PR, Meyer JA, Peters JS, Riley AA, McCarthy BP, Gao M, et al. Characterization of ¹¹C-GSK1482160 for Targeting the P2X7 Receptor as a Biomarker for Neuroinflammation. *J Nucl Med* 2017;58:458.
- <https://adisinsight.springer.com/drugs/800033444>.
- <https://adisinsight.springer.com/drugs/800039286>.
- Recourt K, van der Aart J, Jacobs G, de Kam M, Drevets W, van Nueten L, et al. Characterisation of the pharmacodynamic effects of the P2X7 receptor antagonist JNJ-54175446 using an oral dexamphetamine challenge model in healthy males in a randomised, double-blind, placebo-controlled, multiple ascending dose trial. *J Psychopharmacol* 2020;34:1030–42.
- Timmers M, Ravenstijn P, Xi L, Triana-Baltzer G, Furey M, Van Hemelryck S, et al. Clinical pharmacokinetics, pharmacodynamics, safety, and tolerability of JNJ-54175446, a brain permeable P2X7 antagonist, in a randomised single-ascending dose study in healthy participants. *J Psychopharmacol* 2018;32:1341–50.
- Bhattacharya A, Lord B, Grigoleit J-S, He Y, Fraser I, Campbell SN, et al. Neuropsychopharmacology of JNJ-55308942: evaluation of a clinical candidate targeting P2X7 ion channels in animal models of neuroinflammation and anhedonia. *Neuropsychopharmacology* 2018;43:2586–96.
- Wei L, Syed Mortadza SA, Yan J, Zhang L, Wang L, Yin Y, et al. ATP-activated P2X7 receptor in the pathophysiology of mood disorders and as an emerging target for the development of novel antidepressant therapeutics. *Neurosci Biobehav Rev* 2018;87:192–205.
- Tian M, Abdelrahman A, Weinhausen S, Hinz S, Weyer S, Dosa S, et al. Carbamazepine derivatives with P2X4 receptor-blocking activity. *Bioorg Med Chem* 2014;22:1077–88.
- Hattori M, Gouaux E. Molecular mechanism of ATP binding and ion channel activation in P2X receptors. *Nature* 2012;485:207–12.
- Lewis CJ, Surprenant A, Evans RJ. 2',3'-O-(2,4,6-trinitrophenyl) adenosine 5'-triphosphate (TNP-ATP)—a nanomolar affinity antagonist at rat mesenteric artery P2X receptor ion channels. *Br J Pharmacol* 1998;124:1463–6.
- Virginio C, Robertson G, Surprenant A, North RA. Trinitrophenyl-substituted nucleotides are potent antagonists selective for P2X1, P2X3, and heteromeric P2X2/3 receptors. *Mol Pharmacol* 1998;53:969–73.
- Ase AR, Honson NS, Zaghdane H, Pfeifer TA, Seguela P. Identification and characterization of a selective allosteric antagonist of human P2X4 receptor channels. *Mol Pharmacol* 2015;87:606–16.
- Michel AD, Chambers LJ, Walter DS. Negative and positive allosteric modulators of the P2X(7) receptor. *Br J Pharmacol* 2008;153:737–50.
- Jahangir A, Alam M, Carter DS, Dillon MP, Bois DJ, Ford AP, et al. Identification and SAR of novel diaminopyrimidines. Part 2: The discovery of RO-51, a potent and selective, dual P2X(3)/P2X(2/3) antagonist for the treatment of pain. *Bioorg Med Chem Lett* 2009;19:1632–5.
- Carter DS, Alam M, Cai H, Dillon MP, Ford AP, Gever JR, et al. Identification and SAR of novel diaminopyrimidines. Part 1: The discovery of RO-4, a dual P2X(3)/P2X(2/3) antagonist for the treatment of pain. *Bioorg Med Chem Lett* 2009;19:1628–31.
- Brotherton-Pleiss CE, Dillon MP, Ford AP, Gever JR, Carter DS, Gleason SK, et al. Discovery and optimization of RO-85, a novel drug-like, potent, and selective P2X3 receptor antagonist. *Bioorg Med Chem Lett* 2010;20:1031–6.
- Wang J, Wang Y, Cui WW, Huang Y, Yang Y, Liu Y, et al. Druggable negative allosteric site of P2X3 receptors. *Proc Natl Acad Sci U S A* 2018;115:4939–44.
- Kwon M, Firestein BL. DNA transfection: calcium phosphate method. *Methods Mol Biol* 2013;1018:107–10.
- Zhao WS, Wang J, Ma XJ, Yang Y, Liu Y, Huang LD, et al. Relative motions between left flipper and dorsal fin domains favour P2X4 receptor activation. *Nat Commun* 2014;5:4189.
- Yu Y, Chen Z, Li WG, Cao H, Feng EG, Yu F, et al. A nonproton ligand sensor in the acid-sensing ion channel. *Neuron* 2010;68:61–72.

- [46] Coddou C, Yan Z, Obsil T, Huidobro-Toro JP, Stojilkovic SS. Activation and regulation of purinergic P2X receptor channels. *Pharmacol Rev* 2011;63:641–83.
- [47] Lewis CJ, Evans RJ. Lack of run-down of smooth muscle P2X receptor currents recorded with the amphotericin permeabilized patch technique, physiological and pharmacological characterization of the properties of mesenteric artery P2X receptor ion channels. *Br J Pharmacol* 2000;131:1659–66.
- [48] Bitencourt-Ferreira G, de Azevedo WF, Jr. Homology Modeling of Protein Targets with MODELLER. *Methods Mol Biol* 2019;2053:231–49.
- [49] Larkin MA, Blackshields G, Brown NP, Chenna R, McGettigan PA, McWilliam H, et al. Clustal W and Clustal X version 2.0. *Bioinformatics* 2007;23:2947–8.
- [50] Laskowski RA, Macarthur MW, Moss DS, Thornton JM. Procheck - a program to check the stereochemical quality of protein structures. *J Appl Crystallogr* 1993;26:283–91.
- [51] Shaw DE. A fast, scalable method for the parallel evaluation of distance-limited pairwise particle interactions. *J Comput Chem* 2005;26:1318–28.
- [52] Lomize MA, Pogozheva ID, Joo H, Mosberg HI, Lomize AL. OPM database and PPM web server: resources for positioning of proteins in membranes. *Nucleic Acids Res* 2012;40:D370–6.
- [53] Kaminski GA, Friesner RA, Tirado-Rives J, Jorgensen WL. Evaluation and reparametrization of the OPLS-AA force field for proteins via comparison with accurate quantum chemical calculations on peptides. *J Phys Chem B* 2001;105:6474–87.
- [54] Jorgensen WL, Maxwell DS, TiradoRives J. Development and testing of the OPLS all-atom force field on conformational energetics and properties of organic liquids. *J Am Chem Soc* 1996;118:11225–36.
- [55] Le Guilloux V, Schmidtke P, Tuffery P. Fpocket: an open source platform for ligand pocket detection. *BMC Bioinf* 2009;10:168.
- [56] Yuan JH, Han SB, Richter S, Wade RC, Kokh DB. Druggability assessment in TRAPP using machine learning approaches. *J Chem Inf Model* 2020;60:1685–99.
- [57] Mansoor SE, Lu W, Oosterheert W, Shekhar M, Tajkhorshid E, Gouaux E. X-ray structures define human P2X(3) receptor gating cycle and antagonist action. *Nature* 2016;538:66–71.
- [58] McCarthy AE, Yoshioka C, Mansoor SE. Full-length P2X7 structures reveal how palmitoylation prevents channel desensitization. *Cell* 2019;179(659–70):e13.
- [59] Wang J, Sun LF, Cui WW, Zhao WS, Ma XF, Li B, et al. Intersubunit physical couplings fostered by the left flipper domain facilitate channel opening of P2X4 receptors. *J Biol Chem* 2017;292:7619–35.
- [60] Burnstock G. Purinergic signalling: therapeutic developments. *Front Pharmacol* 2017;8:661.
- [61] Wagner JR, Lee CT, Durrant JD, Malmstrom RD, Feher VA, Amaro RE. Emerging computational methods for the rational discovery of allosteric drugs. *Chem Rev* 2016;116:6370–90.
- [62] Muccino DR, Morice AH, Birring SS, Dicipinigitis PV, Pavord ID, Assaid C, et al. Design and rationale of two phase 3 randomised controlled trials (COUGH-1 and COUGH-2) of gefapixant, a P2X3 receptor antagonist, in refractory or unexplained chronic cough. *ERJ Open Res* 2020;6.
- [63] Dicipinigitis PV. Coming soon: the first-ever drug(s) for refractory chronic cough. *Lung* 2021;199:83–4.
- [64] Coddou C, Stojilkovic SS, Huidobro-Toro JP. Allosteric modulation of ATP-gated P2X receptor channels. *Rev Neurosci* 2011;22:335–54.
- [65] Obrecht AS, Urban N, Schaefer M, Rose A, Kless A, Meents JE, et al. Identification of aurintricarboxylic acid as a potent allosteric antagonist of P2X1 and P2X3 receptors. *Neuropharmacology* 2019;158:107749.
- [66] Wang J, Yu Y. Insights into the channel gating of P2X receptors from structures, dynamics and small molecules. *Acta Pharmacol Sin* 2016;37:44–55.
- [67] Serrano A, Mo G, Grant R, Pare M, O'Donnell D, Yu XH, et al. Differential expression and pharmacology of native P2X receptors in rat and primate sensory neurons. *J Neurosci* 2012;32:11890–6.
- [68] Lee Y, Basith S, Choi S. Recent advances in structure-based drug design targeting class A G protein-coupled receptors utilizing crystal structures and computational simulations. *J Med Chem* 2018;61:1–46.
- [69] Verteramo ML, Stenstrom O, Ignjatovic MM, Caldararu O, Olsson MA, Manzoni F, et al. Interplay between conformational entropy and solvation entropy in protein-ligand binding. *J Am Chem Soc* 2019;141:2012–26.
- [70] Pasqualetto G, Brancale A, Young MT. The molecular determinants of small-molecule ligand binding at P2X receptors. *Front Pharmacol* 2018;9:58.